Biol Cybern (2006) 95:589–605
DOI 10.1007/s00422-006-0127-z

ORIGINAL PAPER

Biological Cybernetics

Early motor development from partially ordered neural-body dynamics: experiments with a cortico-spinal-musculo-skeletal model

Yasuo Kuniyoshi · Shinji Sangawa

Received: 25 September 2006 / Accepted: 19 October 2006 / Published online: 23 November 2006

Abstract Early human motor development has the nature of spontaneous exploration and boot-strap learning, leading to open-ended acquisition of versatile flexible motor skills. Since dexterous motor skills often exploit body-environment dynamics, we formulate the developmental principle as the spontaneous exploration of consistent dynamical patterns of the neural-body-environment system. We propose that partially ordered dynamical patterns emergent from chaotic oscillators coupled through embodiment serve as the core driving mechanism of such exploration. A model of neuro-musculo-skeletal system is constructed capturing essential features of biological systems. It consists of a skeleton, muscles, spindles, tendon organs, spinal circuits, medullar circuits (CPGs), and a basic cortical model. Through a series of experiments with a minimally simple body model, it is shown that the model has the capability of generating partially ordered behavior, a mixture of chaotic exploration and ordered entrained patterns. Models of self-organizing cortical areas for primary somatosensory and motor areas are introduced. They participate in the explorative learning by simultaneously learning and controlling the movement patterns. A scaled up version of the model, a human infant model, is constructed and put through preliminary experiments. Some meaningful motor behavior emerged including rolling over and crawling-like motion. The results show the possibility that a rich variety of meaningful behavior can be discovered and acquired by the neural-body dynamics without pre-defined coordinated control circuits.

Y. Kuniyoshi
ERATO Asada Synergestic Intelligence Project,
The University of Tokyo, Tokyo, Japan

S. Sangawa
Department of Mechano-Informatics,
School of Information Science and Technology,
The University of Tokyo, Tokyo, Japan

Y. Kuniyoshi (✉)
Department of Mechano-Informatics,
School of Information Science and Technology,
The University of Tokyo, Tokyo, Japan
e-mail: kuniyosh@isi.imi.i.u-tokyo.ac.jp

Present Address:
S. Sangawa
Intellectual Property Division, Sony Co., Tokyo, Japan
e-mail: Shinji.Sangawa@jp.sony.com

1 Introduction

The versatility and dexterity (Bernstein 1996) of human motor behavior primarily depend on the high degrees of freedom (DOFs) body and powerful adaptation/learning capability. These two factors conflict with each other. The search space for all possible movements of a complex body is hopelessly large, particularly when dynamics is taken into account (Kuniyoshi et al. 2004). Thus, in humanoid robotics, autonomous acquisition of novel whole-body motor skills has been almost intractable.

Most of the motor learning models proposed to date assume pre-defined motor *primitives*, which are atomic (sometimes parameterized) units of coordinated motor patterns. A trial-and-error type learning model, e.g. reinforcement learning, repeatedly generates and tests combinations of the primitives. Thus it is generally important to define adequate chunk size (over DOFs and time) for the primitives; larger chunks lead to reduced search space dimensionality at the cost of reduced flexibility. Some methodologies such as hierarchical reinforcement

learning (Morimoto and Doya 2001) provides partial solutions. Nevertheless, existing methods require carefully designed initial primitives.

Human babies seem to be able to autonomously explore and acquire a wide range of adequate motor primitives. Quickly accumulating evidences in developmental sciences suggest the large effect of self-driven exploration and learning on the motor and neural development starting as early as the fetal period (Johnson 2005). Thus it is highly plausible that an adequate set of dynamic motion primitives is acquired in the development, which serves as the powerful platform for highly dexterous, flexible and robust human motor behavior.

The ultimate goal of our research program is to reveal the underlying principles of exploration and acquisition of motor primitives in human babies, and extract design principles for versatile adaptive humanoid robots.

Human development is an extremely complex process emerging from tightly coupled physical, genetic, neural and environmental factors. Therefore, divide-and-analyze methodologies will not lead to a correct understanding. In this paper, we take a synthetic methodology in which we construct a minimal model of the target system, let it behave and develop in an environment, compare the results with the target to reveal the basic principles.

In concrete terms, we construct a musculo-skeletal model which captures some of the essential properties of the human body, connect with the minimum model of the central nervous system, namely, the spine, medulla and primary somatosensory and motor cortices. Then we let it behave and learn, and compare the results between different settings and with some characteristics of human motor development. The goal is to find the principles of self-driven exploration and learning that resolves the dilemma of searching for primitives without initial primitives.

2 Explorative dynamics from neural-body coupling

We hypothesize that the explorative capability emerges from the coupled dynamics of the nervous system and the body. In the following, we first discuss the context and then present the core principles.

2.1 Early motor/neural development

A human fetus, only 2 months (8.5–9.5 weeks) after gestation, begins to exhibit spontaneous atypical whole-body motor activity called *generalized movements* (GM) (Kisilevsky and Low 1998). Until 14–19 weeks of gestational age (wk GA), GM continues to be highly active, resting state lasting only 5 min or so. Between 16 and 32 wk GA, the frequency and duration of GM decreases. Approaching the birth, by 40 wk GA, the number of GM decreases but novel unique motor patterns emerge and develop.

The nervous system develops in parallel with the above, while the fetus is continuously engaged in motor activities and development. By only 17.5 days GA, some of the neural axons (of CST: Corticospinal Tract and BST: Bulbospinal Tract) are already formed and reach the lumber vertebrae, possibly carrying some signals between the cortex and spine. By 20 wk GA, CST axons reach target peripheral neurons all over the body. By the same time, the genesis of the muscle spindles (muscle length sensors) is complete (Sarnat (2003)). The most basic mono-synaptic reflex called stretch reflex is complete by 25 wk GA.

The genesis of the brain starts very early on (together with the spine), and mostly completes by around 7 months GA, in the sense that the vast majority of neurons are formed and migrated to appropriate brain regions (Johnson 2005). However, synaptic connections and *representations* of the cortex are another issues. They continue to develop through a long period, as far as adulthood.

To summarize, by around 25 wk GA, all the sensory (spindles), motor (muscles), and neural systems (spine, medulla, cortex) are present and interconnected. And the fetus is actively engaged in GM. Thus it is natural to expect that the sensory–motor information from the motor activity affect the durative neural development. Many evidences support that the neural activity and incoming signals have important effects on brain development (Crair 1999; Johnson 2005; Rakic 1988).

2.2 Neural-body dynamics and CPG

A humanoid body has well over 30 DOFs and its space of possible dynamic motion is astronomically large. However, there are evidences that in some tasks, the global dynamics has a distinct, very simple structure in terms of stable limit cycles (McGeer 1990; Rizzi and Koditschek 1993; Wisse and van Frankenhuyzen 2006), or branching and contraction of state space trajectory bundles with regard to the reachability to the goal (Kuniyoshi et al. 2004), and that humans exploit such structure for easy and robust control of the whole-body motion.

A well known example of neural-body coupling that exploit the natural body dynamics is the CPG driven rhythmic motions. CPG's (Central Pattern Generators) (Grillner et al. 1991) are found in bulbar/spinal circuits of vertebrates that generate coordinated oscillatory motor patterns.

Extensive research have been carried out on CPG's and CPG based motor behavior, including biped walking (Aoi and Tsuchiya 2006; Taga et al. 1991), quadruped walking (Collins and Richmond 1994; Kimura et al. 2001), adaptive locomotion and swimming (Ijspeert 2001), and many others.

The underlying principle of CPG-based motor behavior is called mutual entrainment, in which the coupling of the neural and body (and environment) dynamics co-creates a stable limit cycle attractor (Taga 1994). Typically, careful parameter tuning is required for this. And in its basic form the CPG can create only a single limit cycle behavior. A networked CPG can create and switch between different modes of limit cycle motion (Ijspeert 2001; Pribe et al. 1997), but the parameters and the modes are predetermined (e.g. by manual tuning or using genetic algorithm), and the transition is commanded by an external signal.

Many efforts have been made to incorporate learning techniques (Sato et al. 2002) and a combinatorial architecture (Yang and França 2003). However, the search process is driven and controlled by an external process by means of a goal-directed generate and test principle. Thus, they are not suitable as the model of spontaneous and autonomous exploration, without external specification, for a wide range of dynamical patterns emerging from neural-body coupled dynamics.

To summarize, the mutual entrainment between the CPG and the body (plus environment) dynamics is an important principle of biological motor behavior. However, typical CPG models and learning techniques are not suitable as a model of spontaneous and autonomous nature of early human motor development.

2.3 Coupled chaos system and emergence of order

Coupled map lattice (CML) and globally coupled map (GCM) have been investigated in complex systems science for their rich dynamical properties (Kaneko 1984, 1989, 1990; Kaneko and Tsuda 2001). They are pure mathematical models of coupled multiple chaotic elements represented as Eqs.(1)–(2). In CML, each element is coupled locally, with only adjacent elements in the basic form (1), whereas in GCM each is coupled to all the elements via the *mean field* (2).

$$x^i_{n+1} = (1-\varepsilon) f\left(x^i_n\right) + \frac{\varepsilon}{2}\left\{f\left(x^{i+1}_n\right) + f\left(x^{i-1}_n\right)\right\} \tag{1}$$

$$x^i_{n+1} = (1-\varepsilon) f\left(x^i_n\right) + \frac{\varepsilon}{N}\sum_{j=1}^{N} f\left(x^j_n\right) \tag{2}$$

In the above, x^i_n denotes the internal state of i-th element at time n, N the total number of elements, and ε the connection weight between elements.

For CML and GCM to exhibit rich variety of dynamical structures, $f(x)$ can be chosen from a large class of functions that yield chaotic maps.

When there is no coupling between the elements, i.e. $\varepsilon = 0$, each of them behaves completely independently and chaotically. When coupling is enabled, a variety of dynamical structures emerge depending on the parameters (a, ε); a coherent phase in which all the elements oscillate in a unison, ordered phases with various number of clusters (a cluster is a group of mutually entrained and resonating elements), partially ordered phases with gradually changing configuration of clusters, and completely random (chaotic) patterns.

This phenomenon is essentially caused by a competition of two tendencies embedded in the mathematical model; (1) a tendency to synchronize each other by the effect of the mean-field, and (2) a tendency to take arbitrarily different values due to the nature of chaos dynamics.

2.4 Emergent order out of coupled chaos system

An important finding with GCM is that when its coupling coefficient ε is made spatially variant, i.e. a function $\varepsilon(i)$ of the element index, then the structure of the resonance clusters reflect the distribution of $\varepsilon(i)$ (Kaneko 1994). The elements with large $\varepsilon(i)$ tend to synchronize and form large clusters, and those with small values tend to de-synchronize. This suggests that some external information structure can be imposed on the resonance structure of GCM via $\varepsilon(i)$.

Another important phenomenon in high dimensional chaos is *chaotic itinerancy*, where the system wanders from one *quasi*-attractor to another, getting entrained in each only for a while (Tsuda 1991). This can be interpreted as the functionality of spontaneous exploration for various quasi-stable dynamics.

Another important finding (Matsumoto and Tsuda 1983), called Noise Induced Order, is that when a small amount of noise is input to a chaotic system, suddenly the chaos collapses and the novel ordered dynamics emerges. A relevant finding, called OGY-method, is that a small time-dependent perturbation of a parameter of a chaotic system can convert the chaotic attractor into any possible time-periodic attractor (Ott et al. 1990). Recently, the above line of principles have been demonstrated in various physical systems (Arena et al. 2000).

To summarize, high dimensional chaotic system such as GCM/CML can change its dynamical structure, including the configuration of quasi-attractors, to reflect

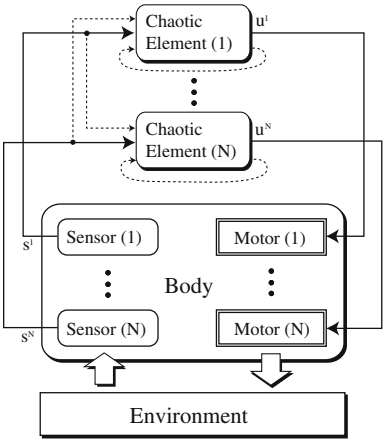

Fig. 1 Chaos coupling through embodiment (adopted from Kuniyoshi and Suzuki 2004)

external information via coupling coefficients and perturbation, and can spontaneously explore for quasi-attractors and get temporarily entrained in them.

2.5 Emergence of coordination from chaos coupling through embodiment

In the context of motor behavior, the rich variety of cluster configuration described above can be interpreted as a variety of *coordination patterns* of multiple motor elements. Each coordination pattern self-organizes (emerges) and has limited self stability due to mutual entrainment among the elements. On the other hand, the coordination patterns change in response to the change of the coupling.

The above interpretation suggests an architecture depicted in Fig. 1. It has multiple chaos elements, each connected with a sensor and motor element. A biological example is a pair of a muscle and spindle, connected to some spinal or bulbar neuron with chaotic property. The multiple sensor-motor units interact with each other through the *physical dynamics* of the body. Thus the units are mutually coupled and form a coupled chaos system. Unlike the original mean field model, this coupling is non-linear and time-varying. The effect of body-environment dynamics is also reflected on the coupling.

Theoretically very little is known about the complex case as the above. However, because the coupling field directly reflects the body-environment dynamics, and because the system has the potential to self-organize attractor dynamics, we believe there is a possibility that the emergent ordered patterns correspond to some meaningful motor behavior exploiting body-environment dynamics. In other words, the system can explore, discover, and get entrained into a variety of embodied dynamics. In a series of experiments with simulated multi DOF robots, we showed the possibility of the system to exhibit such capability (Kuniyoshi and Suzuki 2004).

3 Neural-musculo-skeletal model for spontaneous exploration and learning

In Sect. 2 we proposed that early motor development requires spontaneous exploration and temporary entrainment into natural body-environment dynamics. And we discussed a possibility that such functionality can emerge from a high-dimensional chaotic system whose couplings are made through the embodiment via sensors and motors.

In this section, we show a biologically plausible model that has the above discussed property.

3.1 CPG-musculo-skeletal system as embodied coupled chaos system

Medulla Oblongata (medulla, in short) is a part of the brain stem. It controls important biogenic motor activities such as breathing and heart-beating. These are rhythmic motor patterns, and the circuits that generate such rhythmic patterns are called CPG (Central Pattern Generator). Medulla is also responsible for other rhythmic motor behavior such as walking and chewing. It is important to note that for these rhythmic bodily movements, the spinal circuits, musculo-skeletal system, sensory organs such as spindles, and body-environment interaction are all involved to create the global dynamical system.

Typically, CPG's create cyclic motor patterns, but sometimes they contain chaotic pattern components. For example, respiration patterns in neonates have chaotic components (Small et al. 1999). This, and many other evidences suggest that the CPG circuits in medulla has the capability of generating chaos.

A computational model of CPG that can generate both periodic and chaotic patterns has been reported by Asai et al. (2000, 2003). They assumed a CPG model represented as a pair of weakly coupled BVP (Bonhöffer van der Pol) oscillators as the following.

$$\left.\begin{aligned} \frac{dx_1}{dt} &= c\left(x_1 - \frac{x_1^3}{3} - y_1 + z_1\right) + \delta(x_2 - x_1) \\ \frac{dy_1}{dt} &= \frac{1}{c}(x_1 - by_1 + a) + \varepsilon x_2 \end{aligned}\right\} \quad (3)$$

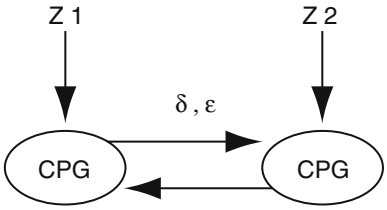

Fig. 2 Coupled CPG model (Asai et al. 2000, 2003). $z1$, $z2$: control signals, δ, ε : coupling constant

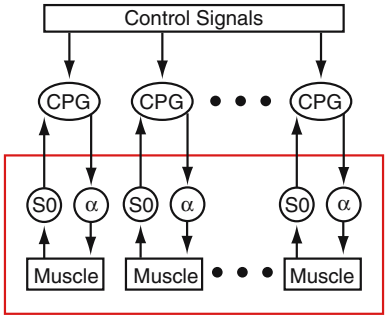

Fig. 3 Body coupled CPG model. CPG: a BVP unit. α:α motor neuron in the spinal cord. S0: afferent (sensory) interneuron in the spinal cord. *Muscle* includes a muscle and a spindle (muscular sensory organ)

$$\left.\begin{aligned} \frac{\mathrm{d}x_2}{\mathrm{d}t} &= c\left(x_2 - \frac{x_2^3}{3} - y_2 + z_2\right) + \delta(x_1 - x_2) \\ \frac{\mathrm{d}y_2}{\mathrm{d}t} &= \frac{1}{c}(x_2 - by_2 + a) + \varepsilon x_1 \end{aligned}\right\} \tag{4}$$

Here, the first pair of equations (3) defines one oscillator, and the second pair (4) defines the other. The two oscillators are coupled via two coefficients δ, ε. z_1, z_2 are externally fed control signals. A graphical description is given in Fig. 2.

Asai et al. discovered that when $z_1 = z_2$ the CPG generates a limit cycle pattern, but when $z_1 \neq z_2$ a complex chaotic pattern emerges. Thus, the BVP oscillator can play both role of a typical cyclic CPG and a chaos element, depending on the external input.

Relating the above model with our idea of chaos coupling through embodiment in Sect. 2.5, we define the core neuro-musculo-skeletal organization whose essential part is depicted in Fig. 3.

In this model, each CPG neuron in medulla is connected to a muscle via an α motor neuron and an afferent interneuron in the spinal cord. The α neuron commands muscular contraction and the muscle length is sensed by a spindle connected to the afferent interneuron.

Each CPG neuron is modeled by the following BVP equation.

$$\left.\begin{aligned} \frac{1}{\tau}\cdot\frac{\mathrm{d}x}{\mathrm{d}t} &= c\left(x - \frac{x^3}{3} - y + I_{\mathrm{control}}\right) + \delta(I_{S0} - x) \\ \frac{1}{\tau}\cdot\frac{\mathrm{d}y}{\mathrm{d}t} &= \frac{1}{c}(x - by + a) + \varepsilon I_{S0} \end{aligned}\right\} \tag{5}$$

Here, the constants are set as $a = 0.7$, $b = 0.675$, $c = 1.75$, $\delta = 0.013$, $\varepsilon = 0.022$. The time constant $\tau = 3.5$ is used for the experiments with the 1-joint model ($\tau = 5.0$ for the infant model in Sect. 5). The initial value of x is set to a random value within the range $-0.1 \leq x \leq 0.0$.

We assume *no* internal connections among the multiple CPG neurons. Nevertheless, they are coupled through physical interactions through the body (Fig. 3). A simplest case is with an antagonistic pair of muscles where the contraction of one muscle stretches the other muscle. Due to the spring property of the stretched muscle, the effect from its own α motor neuron and the other muscle are mixed together and sensed by the spindle.

The assumption of no internal connections is an extreme hypothesis which may deviate from biological reality. However, we think it is important to start with this extreme case in order to show that coordinated motor patterns can emerge without pre-defined coordination circuit.

In (5), I_{control} is a control signal from higher nervous centers. And I_{S0} is defined using O_{S0}, the output of S0, as the following.

$$I_{S0} = -40 \cdot O_{S0} + 20 \tag{6}$$

Here, and throughout the paper, all neural signals are normalized to dimensionless values defined as the following.

$$150[\mathrm{pulse/s}] = 100[\mathrm{nA}] = 1 \tag{7}$$

When a neural signal has a dimensionless value 1, it means either real current 100 nA or real pulse frequency $150\,\mathrm{s}^{-1}$. This is because our muscle model (described later) has activity value 1 on an input pulse train of $150\,\mathrm{s}^{-1}$, and our spinal neuron model outputs a pulse train at $150\,\mathrm{s}^{-1}$ when fed 100 nA as input. In short, all neural signal value measures are normalized to a unit muscular activity.

The output of each CPG neuron O_{CPG} is defined as the following.

$$O_{\mathrm{CPG}} = 0.25 \cdot x + 0.34 \tag{8}$$

In our experiments, O_{CPG} mostly takes the value within the range $-0.1 < O_{\mathrm{CPG}} < 0.9$.

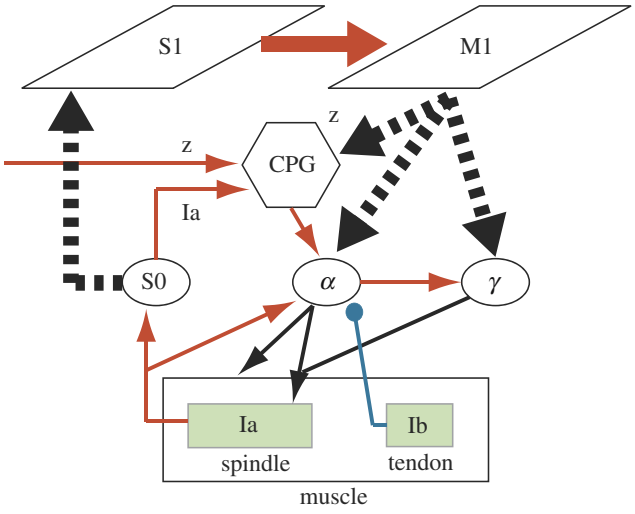

Fig. 4 Model of neural circuit. CPG: CPG neuron, *S*1: primary somatosensory area, *M*1: primary motor area, α: α motor neuron, γ: γ motor neuron, S0: afferent interneuron. *Arrow* and *filled circle* represent excitatory and inhibitory connection, respectively. *Thick broken lines* represent all to all connections with plasticity

3.2 Cortico-medullar-spinal-musculo-skeletal system - overview

Based on the core model of emergent explorative dynamics above, we propose an integrated model of explorative motor learning with minimum components. Figure 4 shows the overall structure of the model. It consists of network models of the primary somatosensory (S1) and primary motor (M1) areas of the cerebral cortex, the CPG model of medulla (Sect. 3.1), the efferent (α and γ neurons) and afferent (S0) spinal neurons, and the muscle with sensory organs (Ia: spindle, Ib: tendon).

The cortical areas S1 and M1 are modeled as self-organizing neural networks. The connections between the cortical areas and the medullar-spinal circuit have plasticity modeled with Hebbian learning.

While the overall neural-musculo-skeletal system generate exploratory bodily movements, the neural system learns the sensory–motor patterns. If some coherency emerges in the sensory–motor patterns due to the global neural-musculo-skeletal entrainment, it will be captured as stable maps in the self-organizing cortical area models.

There is a past work on modeling self-organizing motor maps coupled with simulated robotic arms (Chen 1997; Goodall et al. 1997). Our cortical model is partially based on their work. A major and critical difference is that their model does not have CPG's or musculo-skeletal model, ignoring the essential effect of body dynamics, and that the model assumes random noises for driving the body while learning.

The output from the primary motor cortex M1 is summed up with a preset tonic input I_{test} and fed into the CPG neuron of (5). In some of the experiments described later, the M1 output is disabled and only I_{test} is fed, for comparative purposes.

$$I_{\text{control}} = \begin{cases} I_{\text{test}} + I_{M1} & \text{(when M1 affects CPG.)} \\ I_{\text{test}} & \text{(when M1 does not affect CPG.)} \end{cases} \tag{9}$$

In the following sections, the details of each component will be given.

3.3 Muscle Model

The muscles play a very important role in the emergence of explorative motor patterns as discussed in Sect. 3.1. Their property constitutes an important component of embodiment that shape the interaction dynamics.

After a careful comparison of modern models (He et al. 2001; Shue and Crago 1998), we adopted the model by He (He et al. 2001) which is based on Hill's equations (Hill 1938). It is simple yet accurate enough, and consistent with the sensory organ models and the spinal circuit models proposed by the same author, which are also adopted in our work.

The model has two components; (1) muscle activity dynamics, and (2) muscle mechanics.

The muscle activity dynamics is defined as follows.

$$\frac{dq}{dt} = 18.8496(m - q) \tag{10}$$

$$u = \frac{q^2}{30^2 + q^2}$$

$$\frac{da}{dt} = 22(1 - 0.51a)^2(u - a) \tag{11}$$

Here, m denotes the pulse frequency (s^{-1}) from the α motor neuron. Equation (10) defines the calcium dynamics, where q is measured in s^{-1}. Equation (11) defines a nonlinear muscle activation dynamics, where u, a are dimension-less numbers. The maximum value of activation is $a = 1$.

He's model of muscle mechanics assumes a particular natural length (0.05 m) and particular maximum contraction force (100 N) of the target muscle. In order to handle various muscles, we define a normalized muscle length l ($l = 1$ for the natural length of the muscle). The contraction force is also normalized using the isometric maximum contraction force $F_{\max}$ N which depends on the cross-section of the target muscle. Thus, the following equation holds between the actual muscle contraction force F (N) and the normalized contraction force $\bar{F}$.

$$F = F_{\max} \cdot \bar{F} \tag{12}$$

$\bar{F}$ consists of normalized active contraction force $\bar{F}_{\text{act}}$ and normalized passive contraction force $\bar{F}_p$.

$$\bar{F} = \bar{F}_{\text{act}} + \bar{F}_p \tag{13}$$

And $\bar{F}_{\text{act}}, \bar{F}_p$ are defined as follows.

$$\bar{F}_{\text{act}} = a \cdot f_l(l) \cdot f_v(v) \tag{14}$$

$$\bar{F}_p = \frac{f_p(l) + B_p(l) \cdot v}{100} \tag{15}$$

In the above, v denotes a normalized contraction velocity.

Further details including the definitions of the variables and the parameters are given in the Appendix.

3.4 Spindle and Golgi tendon organ model

Muscle spindles are embedded in (extrafusal) muscle fibers and activated when the muscle is stretched. Group Ia afferent neurons of a spindle respond to the stretch and its velocity, sending signals to the spinal cord.

The Ia signals are monosynaptically transmitted to an α motor neuron, which commands the muscle to contract. This is called stretch reflex, and has the effect of maintaining the constant muscle length.

Inside a spindle, there are (intrafusal) muscle fibers which are activated by incoming signals from γ motor neurons in the spinal cord, which mechanically modulate the sensitivity of the spindle. This is used by the higher nervous centers to override the effect of stretch reflex. By activating both the α and γ motor neurons, voluntary movement can be generated.

There are another type of afferent neurons (Group II) in the spindle. But since they are not responsive to dynamic changes, we omit them from our model for simplicity.

The Golgi tendon organs are embedded in the tendons at both ends of a muscle, and sense the muscular tension. The Group Ib afferent neurons of the tendon organs transmit the signals via inhibitory connection to the α motor neuron in the spinal cord. This feedback loop has the effect of maintaining a constant muscular tension.

3.4.1 Spindle model

We adopt the spindle model by He et al. (2001).

Let x (m) be the (extrafusal) actual muscle length, y (m) the intrafusal muscle fiber length, and z (m) the length of sensor part of the spindle, then anatomically $x = y + z$. Therefore, the following holds.

$$\dot{z} = \dot{x} - \dot{y} \tag{16}$$

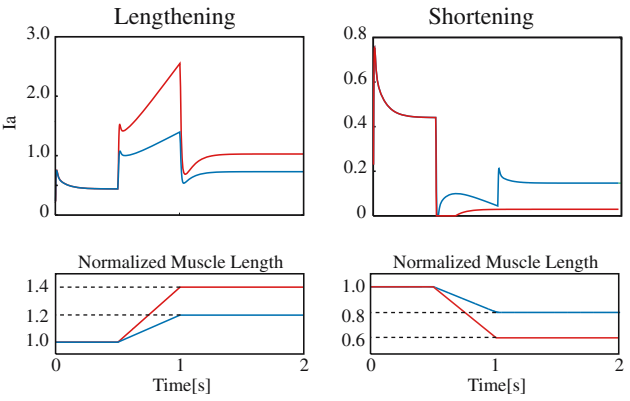

Fig. 5 Response of muscle spindle against muscle lengthening and shortening. Two stimuli: a larger step in *red*, and a smaller step in *blue*. Ia is dimensionless value

The details of how to compute z is given in the Appendix.

I_a (pulse/s), the output of the spindle, is computed by putting the above obtained z through the following transfer function. Some examples of the computed spindle response are shown in Fig. 5.

$$\frac{I_a(s)}{z(s)} = 320 \times 10^3 \cdot \frac{(1 + s/7.23)(1 + s/74.07)}{(1 + s/12.46)(1+s/123.28)(1+s/250)} \tag{17}$$

3.4.2 Golgi tendon organ model

We adopt the Golgi tendon organ model by He et al. (2001). The output I_b (nA) of a tendon organ for a normalized muscle contraction force $\bar{F}$ is obtained via the following transfer function.

$$\frac{I_b(s)}{\bar{F}(s)} = \frac{(1 + s/0.15)(1 + s/1.5)(1 + s/16)}{(1 + s/0.2)(1 + s/2)(1 + s/37)} \tag{18}$$

3.5 Dynamics of spinal neurons

The spinal neurons in Fig. 4, α, γ, and S0, are modeled by the following transfer function (He et al. 2001).

$$\frac{o(s)}{i(s)} = \frac{1.5 \cdot \left(1 + s/33 + (s/33)^2\right)}{1 + 2(s/58) + (s/58)^2} \tag{19}$$

Here, i (nA) denotes an input signal, and o (pulse/s) the output. The range of both signals are constrained in between 0 and 1.

3.6 Somatosensory and motor area models

The model of S1 and M1 is based on Chen's work (Chen 1997; Goodall et al. 1997). It consists of self-organizing

maps with continuous dynamics, a variant of Kohonen's model (Kohonen 1997).

We assume all to all connections for S0 to S1, and M1 to CPG, α and γ. All these connections are plastic with Hebbian learning. This again may deviate from biological reality. In human neural development, it is much more plausible to assume genetically biased coarse localization. However, in order to understand the degree and the content of such genetic bias, we think it is necessary to start with a completely uniform topology and observe what kind of structure emerges through leaning and self organization. After such study, we can investigate various additional constraints and predispositions.

3.6.1 S1 model

The neurons on S1 are arranged in a faveolate structure on a plane (Fig. 6). Each neuron is connected with six adjacent ones bi-directionally with fixed connection weights. Each neuron also takes input from all of the S0 neurons in the spinal cord.

Let us_i denote the potential of neuron i, then the neuron dynamics is defined as the following.

$$\frac{\mathrm{d}us_i}{\mathrm{d}t} = 40.0 \cdot \left(-4.0 \cdot us_i + \frac{\prod_{j \in S0} \mathrm{in}_{ij}}{\sum_{k \in S1} \prod_{j \in S0} \mathrm{in}_{kj}} + \sum_{k \in S1} \mathrm{inn}_{ik} \right) \tag{20}$$

$$\mathrm{in}_{ij} = \begin{cases} 1 - |x_j - w_{ij}| & (|x_j - w_{ij}| < 1.0) \\ 0 & (|x_j - w_{ij}| \geq 1.0) \end{cases} \tag{21}$$

$$\mathrm{inn}_{ik} = 0.5 \cdot ys_k \tag{22}$$

Here, inn_{ik} denotes an input from adjacent neuron k, x_j the output of S0 neuron j, w_{ij} the connection weight from S0 neuron j to S1 neuron i.

The second term of (20) has the effect of competition among the inputs. The normalization over the entire neural plane forces the inputs to compete in terms of closeness to the associated input weight. In essence this is the same principle as in the Kohonen map.

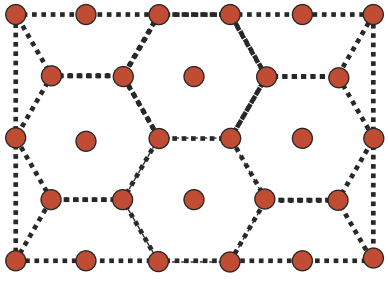

Fig. 6 Faveolate structure of S1 and M1

The output ys_i of S1 neuron i is defined below.

$$ys_i = \begin{cases} 1.0 & (us_i \geq 1.0) \\ us_i & (1.0 > us_i > 0.0) \\ 0.0 & (0.0 \geq us_i) \end{cases} \tag{23}$$

The learning rule for S0–S1 connection weights is the following.

$$\frac{\mathrm{d}w_{ij}}{\mathrm{d}t} = \eta ys_i (x_j - w_{ij}) \tag{24}$$

The initial value of w_{ij} is a random number within $0.0 \leq w_{ij} \leq 0.2$, and η has a constant value of 0.1.

3.6.2 M1 model

M1 has the same number of neurons arranged in the same topology as S1. Each M1 neuron takes inputs from the S1 neurons at the corresponding site and the adjacent six sites. M1 neurons are also fully (all to all) connected to CPG, α, and γ neurons.

Let um_i the potential of M1 neuron i, then the neuron dynamics is defined as follows.

$$\frac{\mathrm{d}um_i}{\mathrm{d}t} = 40.0 \cdot \left(-um_i + 0.2 \cdot \left(ys_j + \sum_{k \in S1} ys_k \right) \right) \tag{25}$$

Here, ys_j denotes the output of S1 neuron j at the site corresponding to M1 neuron i, and ys_k the output of S1 neurons adjacent to S1 neuron j.

The output ym_i of M1 neuron i is um_i but constrained in the same way as (23).

The input in_l to CPG neuron l from M1 neurons is defined as follows.

$$\begin{aligned} \mathrm{in}_l &= \sum_{i \in M1} \bar{w}_{li} \cdot ym_i \\ \bar{w}_{li} &= \frac{w_{li}}{\sum_{i \in M1} w_{li}} \end{aligned} \tag{26}$$

The input to α and γ neurons from M1 neurons are defined likewise.

The connection weights to CPG, α, and γ are updated using the same learning rule as (24). Note that CPG neuron output is constrained between 0 and 1 when computing the rule.

3.7 Lateral organization and corpus callosum

Human cerebrum has left and right hemispheres connected by a bundle of fibers called *corpus callosum*. Each hemisphere controls the other side of the body. Accordingly, the spinal fibers are also grouped into two sides.

In our experiments with a simulated human infant body, we assume the above lateral organization of the

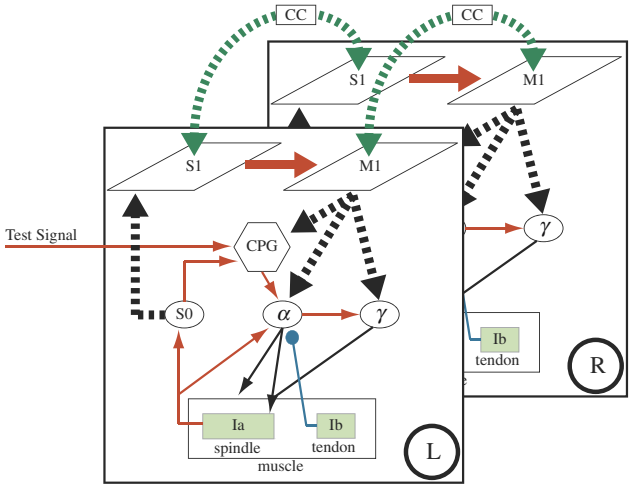

Fig. 7 Lateral organization of the nervous system. *CPG*: CPG neuron, *S1*: primary somatosensory area, *M1*: primary motor area, *CC*: corpus callosum, α: α motor neuron, γ: γ motor neuron, *S0*: afferent interneuron. *Arrow* and *filled circle* represent excitatory and inhibitory connection, respectively. *Thick broken lines* represent all to all connections with plasticity

nervous system. As shown in Fig. 7, we construct left and right nervous systems. And we connect the left and right cortical models with the model of corpus callosum.

As a model of corpus callosum, we define excitatory and plastic full connections between the left and right S1's, and likewise for the M1's. The signal transmission from one cortical area to the other side is defined in the same way as (26). And the learning rule for the connections is defined in the same way as (24).

3.8 Delays and gains

As we are interested in the overall dynamics of the model, proper setting of delay parameters are important. Figure 8 shows the delay and gain parameters determined for the overall neural connections.

For adult spinal circuits, Lin and Crago (2002) estimated important delay parameters; 10 ms delay in the transmission from the α neuron to the muscle fiber, and 5 ms delay in that from the spindle or Golgi tendon organ to the α motor neuron.

However, in fetuses and neonates, the stretch reflex delay is longer than that of adults (Hakamada et al. 1988; Issler and Stephens 1983), amounting to 20 ms instead of 15 ms. Thus, we estimate that the transmission delay from the sensory organs to the α motor neuron is 10 ms, which is 5 ms longer than that of adults.

In adults, the onset of cortical response (of primary somatosensory area 3b) to a cutaneous sensory stimulus is about 15 ms (Inui et al. 2004). This value can be adopted as the afferent transmission delay from the periphery to the cortex. However, in fetuses and neonates, the delay should be much larger because of the immature myelination of the CST (Cortico-Spinal Tract) and BST (Bulbo-Spinal Tract) which starts at about 30 wk GA (Sarnat 2003). We define the delay D_{LongRoot} for CST and BST to be 50 ms. Unfortunately, we could not find any reliable report on the exact amount of the delay in fetuses. Therefore the number we defined is only an estimation. Based on the above considerations, we define the delay parameters in Fig. 8.

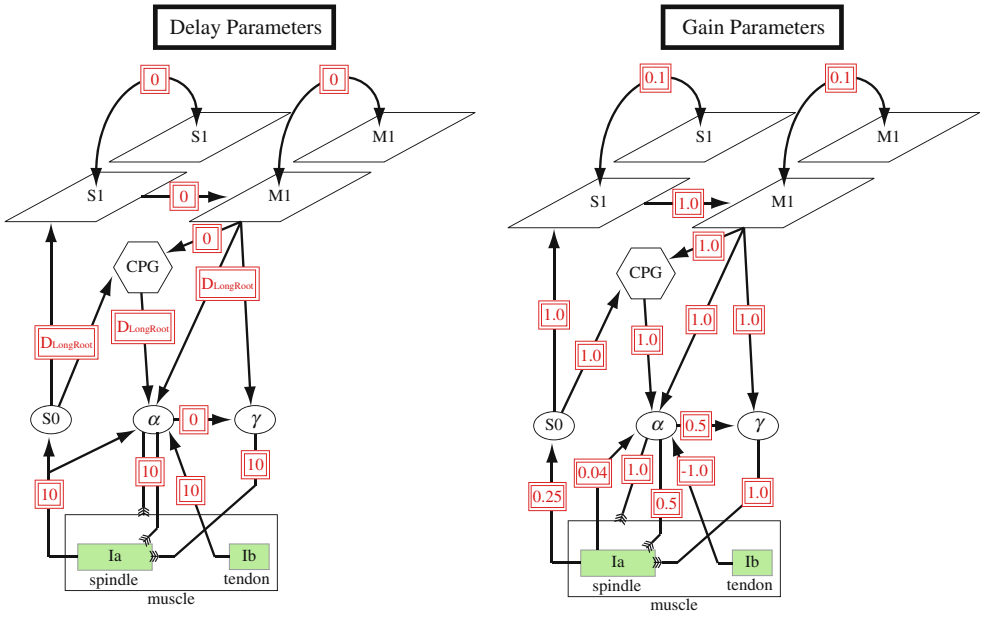

Fig. 8 Delays and connection gains of neural circuit model. *Left* figure represents delays. *Numbers* in squares represent time delays in milliseconds. *Right* figure represents gains

In order to determine the gain parameters along the spinal reflex circuits, we tested our implementation of the neural system for stretch reflex and compared the quantitative results with the other report (He et al. 2001). The other gain values are determined by adjusting the signal range to an appropriate one where necessary. Note that all the connections higher than the spinal cord level are set to 1.0 except for the corpus callosum. So there is no arbitrary parameter tuning. The gain of corpus callosum is set lower in order to avoid meaningless saturating activity. Note also that all cortical connection weights are updated by learning.

4 Experiments with 1-joint model—exploration and learning

We expect that the above described neural-body system has the capability of spontaneously generate complex exploratory movements as well as partially stabilizing on some ordered movement patterns exploiting the natural body dynamics. We also expect that the cortical models can acquire some ordered maps of the body structure which are effective for generating ordered movements. In order to test these assumptions and find appropriate conditions, we first define a very simple musculo-skeletal system and carry out experiments under several different conditions.

4.1 1-Joint body model

As the simplest body model with multiple coordinating elements, we define a 1-joint link system with multiple muscle fibers, shown in Fig. 9.

The body consists of two cylindrical rigid objects (links) connected with a free (spherical) joint that can bend freely in any direction up to 30° from the vertical line. Each link (cylinder) has diameter 0.05 m and height 0.1 m with density 1,000 kg/m^3. The lower link is fixed to the ground. Twelve muscle fibers connect the upper and the lower link. The muscles are placed with equal spacing around the perimeter of the links. The natural length of the muscles are all set to 0.1 m and the maximum contraction force to 100 N. The simulation of physical dynamics is carried out using ODE (Open Dynamic Engine)(R. Smith, http://opende.sourceforget.net/ode.html).

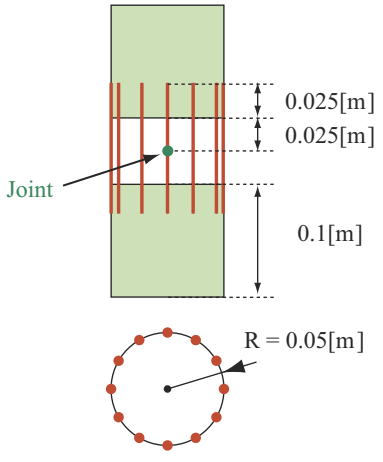

Fig. 9 Homogenous link model

The neural system for the 1-joint model (Fig. 4) has no lateral structure. It has 12 CPG, α, and γ neurons, each connected to one muscle fiber. S1 and M1 has $20 \times 20 = 400$ neurons each. And the delay is set as $D_{\text{LongRoot}} = 70$ ms. All the other parameters are given in Sect. 2.

4.2 Experiments with no cortical control

First, we disable the M1 output, i.e. the gains for M1 to CPG, α, γ signal transmissions are all set to 0.

Concerning the tonic input to the CPG neurons, I_{M1} in (9) is 0. For I_{test}, we tested various cases:

1. Uniform: five cases with different values $I_{\text{test}} = 0.2, 0.4, 0.6, 0.8, 1.0$.
2. Non-uniform: three cases with $I_{\text{test}} = (0.4, 0.6), (0.2, 0.8), (0.0, 1.0)$.

In the above non-uniform case, the CPG neurons connected to the three muscles at 120° spacing (Fig. 10) are fed larger I_{test} values. In the above description, the higher of each pair of numbers is fed to the three particular neurons, and the lower is fed to the rest.

In the following presentation of the results, the movement trajectories of the center of mass of the upper link are given. They are represented as the projection onto the horizontal plane with $x - y$ coordinates (Fig. 11).

The resulting trajectories for simulation time period 1,000 s $\leq t <$ 1,250 s are shown in Fig. 12.

For $I_{\text{test}} = 0.2$, there is almost no movement (note the scale of the axes). For $I_{\text{test}} = 0.4$, $I_{\text{test}} = 0.8$, and $I_{\text{test}} = 1.0$, the trajectories are perfect limit cycles. $I_{\text{test}} =$

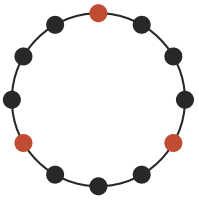

Fig. 10 Non-uniform CPG inputs. Larger I_{test} is fed to the three CPG's corresponding to the three muscles

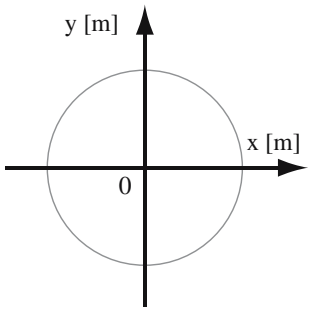

Fig. 11 Coordinate system representing the COG position of upper part of link model

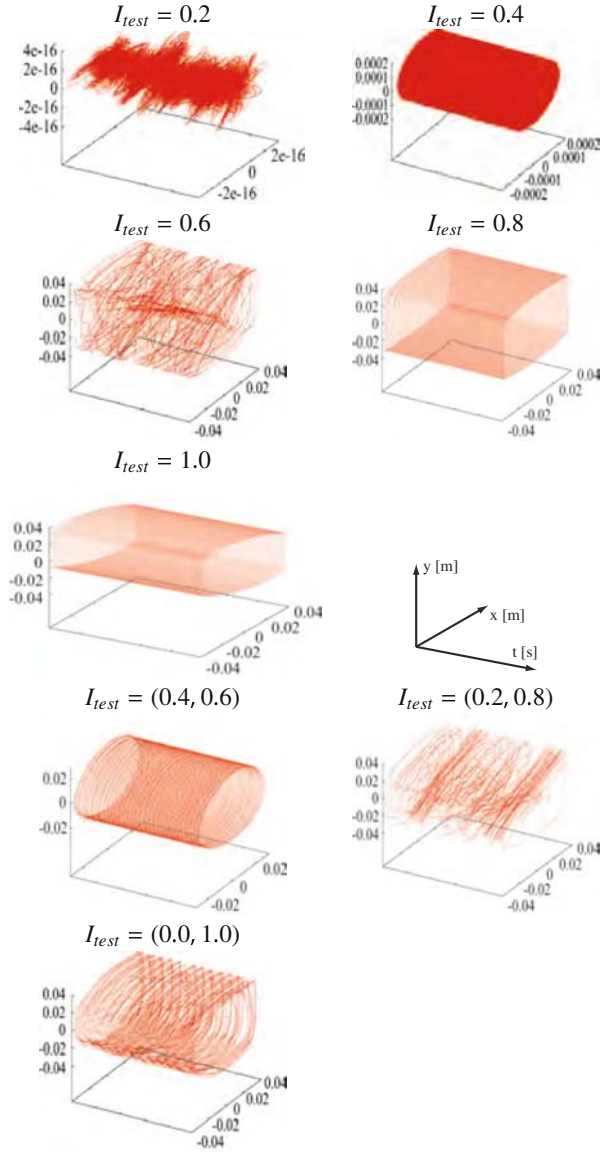

Fig. 12 Trajectories of the upper link of the homogeneous body model. (1,000 s $\leq t <$ 1,250 s)

$(0.4, 0.6)$ and $I_{\text{test}} = (0.0, 1.0)$ also generated limit cycles but with longer periods. It is important to remember that there is absolutely no internal connections between each neural circuit for the individual muscle. The cortical output is disabled (passively learning), and the cross-talks in the cortical models do not affect the movement generation. Therefore the limit-cycle behavior is an emergent pattern from the CPG's interacting with each other through the embodiment.

Non-periodic complex trajectories were observed in two cases; $I_{\text{test}} = 0.6$ and $I_{\text{test}} = (0.2, 0.8)$, which are further investigated. Long term behaviors of these cases are shown in Fig. 13. The uniform case behavior turns into a limit cycle with almost one dimensional oscillation at about $t = 6{,}800$ s and never resumed (observation made until $t = 15{,}000$ s). The non-uniform case behavior continues to be highly complex throughout the experimental period.

Although the uniform case eventually reduced into a limit cycle, it is interesting to note that even though the body and the signals are all homogeneous and uniform, the system still exhibits complex behavior for a long duration. This is due to the non-linear responses of the muscular spindles. They are very sensitive to the normalized muscle contraction velocity as well as the length, and has strongly non-linear responses (Fig. 5). When the upper link is being tilted, each muscle contracts/stretches at a different normalized velocity, i.e. the temporal rate of change of the ratio of the length to the natural length. Therefore the sensory input signals to the CPG neurons become non-uniform, causing the embodiment-coupled CPG neurons to generate chaotic signals.

The results of cortical self organization for the above two cases after the experiments are shown in Fig. 14. The map colors indicate the muscle to which each neuron has the maximum connection weight.

In the uniform case ($I_{\text{test}} = 0.6$), the map is clearly segregated. For each segregated area in S1, the corresponding M1 area codes the antagonistic muscle. This suggests that the cortical model has acquired simple oscillatory movement primitives with alternative activation of antagonistic muscles. The problem with the maps is that they are too simplistic, coding only a few muscles.

In the non-uniform case ($I_{\text{test}} = (0.2, 0.8)$), most part of the map represent the muscles on only one side of the body. Again, the maps are too simplistic, in a different way. The reason for this is that the cortical neurons had little chance to learn correlational structures because the movement was always highly complex, and had very little ordered patterns.

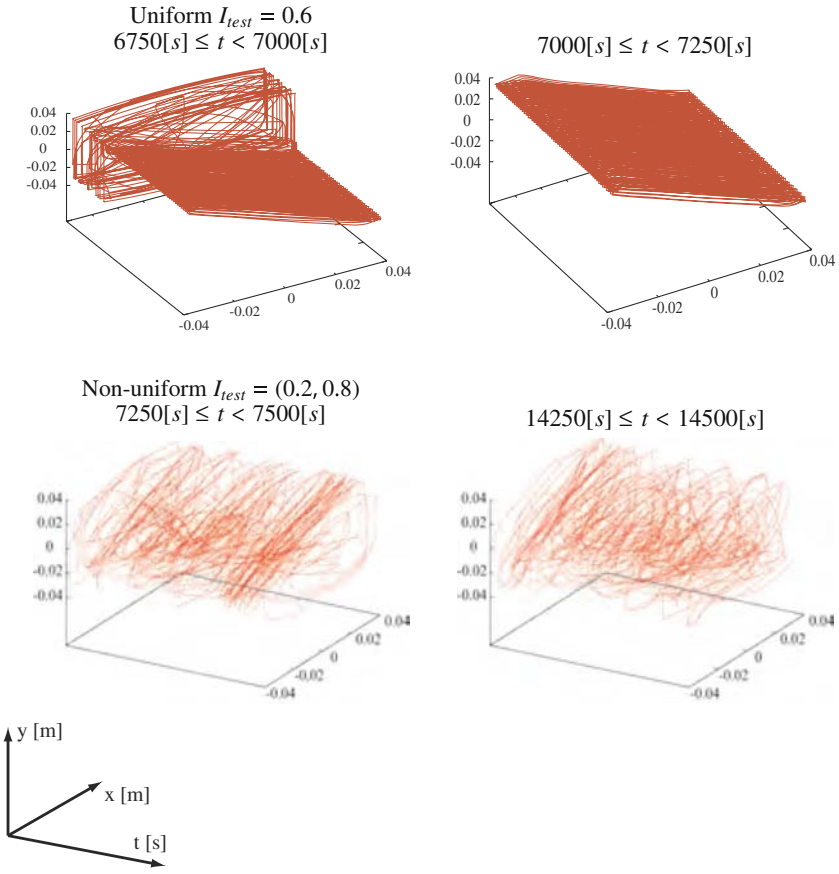

Fig. 13 Characteristic parts of the trajectories of homogeneous body model

These results suggest that the desired behavior should have partially ordered patterns, a mixture of ordered and complex movements.

4.3 Heterogeneous body model

In the above experiments, the body model is perfectly symmetric and homogenous about the vertical axis. On the contrary, real biological bodies are full of asymmetry and heterogeneity. In order to investigate the effect of such factors, we add a slight modification to the 1-joint model.

In the heterogeneous body model, the three muscles at 120° intervals are made shorter (0.07 m) than the other, as shown in Fig. 15. Other parameters are kept the same as the homogeneous one.

First, the same set of experiments with various uniform I_{test} signals have been carried out. We omit the non-uniform signal cases because they are not meaningful for the heterogeneous body model. The results for the period of 1,000 s $\leq t <$ 1,250 s are almost exactly the same as those in Fig. 12 with some scaling and translation in $x - y$ plane, and hence omitted here.

Likewise the previous experiment, the case with $I_{\text{test}} = 0.6$ exhibited a complex trajectory. And we carried out a long-term ($t <$ 15,000 s) experiment on this case.

We found an interesting behavior shown in Fig. 16. The initially complex movement reduced into a low dimensional limit cycle, but then soon (about 250 s) after that, a large amplitude movement with partial order appeared. This behavior may correspond to the chaotic itinerancy discussed in Sect. 2.4. Moreover, a close observation reveals that the complex part (3,000 s $\leq t <$ 3,250) is actually partially ordered, with some periodic parts and some chaotic parts.

The self-organized cortical maps are shown in Fig. 17. The M1 map is quite well segregated into multiple regions representing all the muscles, although some muscles are assigned much smaller regions than the others. Comparing the S1 and M1 patterns, the correspondence is not simplistic as in Fig. 14; one muscle region of S1 corresponds to multiple muscle regions of M1, and vice

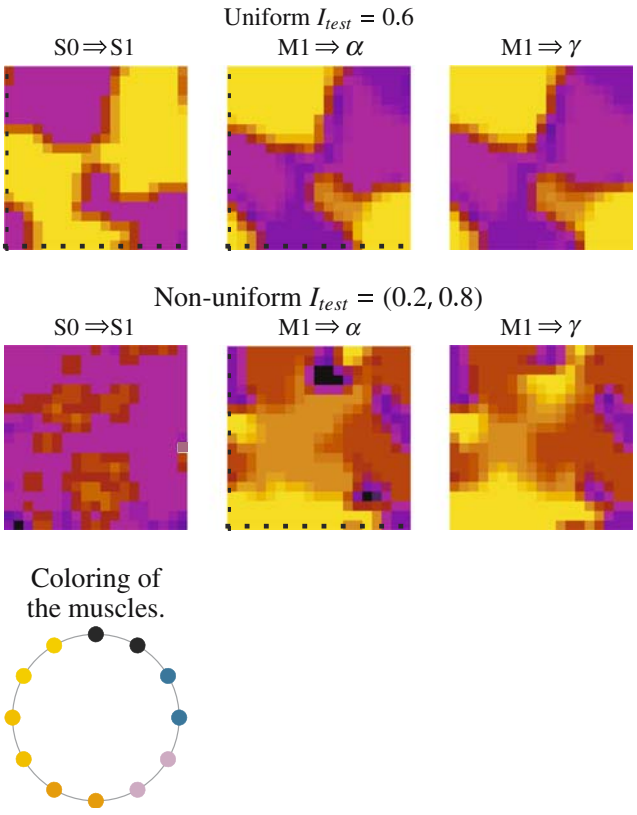

Fig. 14 Self-organization maps of homogeneous body model

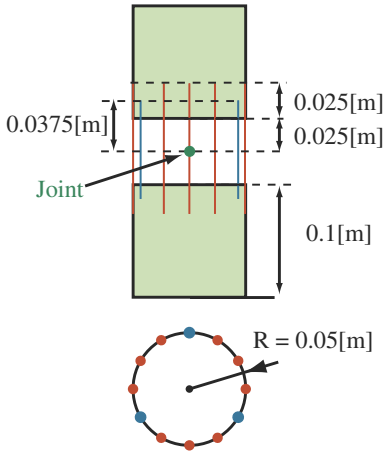

Fig. 15 Heterogeneous link model

versa, suggesting that they code various combinations of muscle coordination patterns.

The above result suggest that the complex embodiment facilitates the neural system for effective exploratory dynamics and learning.

4.4 Learning cortex in the loop

Finally, we investigated about the effect of cortical output. In the same setting as the above, with the heterogeneous body with a uniform input $I_{\text{test}} = 0.6$, the cortical output gains for M1 to CPG, α, γ are set to 1. Now the inputs to the CPG neurons follow the second equation of (9), i.e. summation of M1 output and I_{test}.

A long term experiment ($t < 15{,}000$ s) is carried out. The characteristic trajectories are shown in Fig. 18. After a long period of complex movements with partial order ($t < 9{,}000$s), the movement turned into a perfect limit cycle.

The resulting cortical maps are shown in Fig. 19. They have complex segregated patterns with regions corresponding to every muscle with comparable areas. And the pattern correspondence between S0 and S1 is complex, suggesting the acquisition of a variety of motor primitives.

Even though the trajectory eventually reduced into a perfect limit cycle, the situation is very different from the case with homogeneous body with uniform input (Fig. 13). Here, the cortical map is well organized, actively participating in the movement generation, and the amplitude of oscillation stays large.

What is happening here is the following: As the cortical maps learn the movement patterns, the S0 to M1 pathway resonates with the physical oscillation of the body, actively commanding appropriate muscles to contract. This results in enhanced spindle responses. It has the effect of leveling up the initially incoherent Ia signals (due to different muscle length) to a coherent state. This effectively makes the same situation as the case with the homogeneous body and uniform high level input ($I_{\text{test}} = 0.8$, $I_{\text{test}} = 1.0$ in Fig. 12). This phenomenon may correspond to the *freezing* of DOFs observed in early human motor development (Taga et al. 1999).

5 Experiments with a baby model—emergent behavior

The above experiments suggest the potential capability of the proposed system to explore and learn various motor patterns exploiting embodiment, and to simulate early motor development of humans.

We have constructed a musculo-skeletal model of an infant and carried out a series of experiments. This is an ongoing research and we present partial preliminary results in this paper.

5.1 Body model

The skeletal model (Fig. 20) consists of cylindrical or spherical body segments, connected to each other with constrained joints. We defined 19 segments, omitting the detailed structures such as fingers and the face. Size, mass, and moment of inertia of each segment are deter-

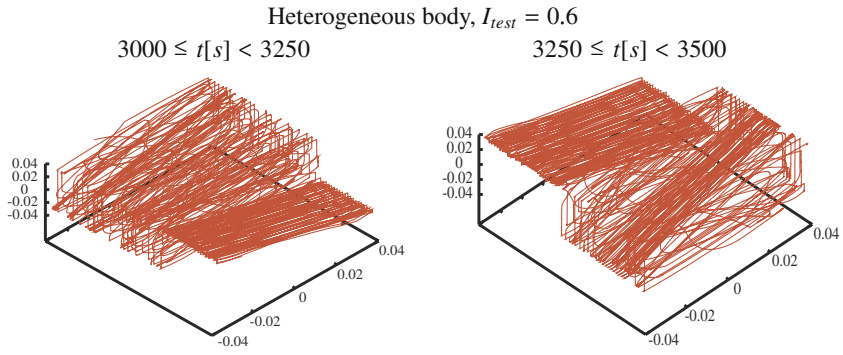

Fig. 16 Characteristic trajectories of heterogeneous body model. Same coordinate system as previous figures

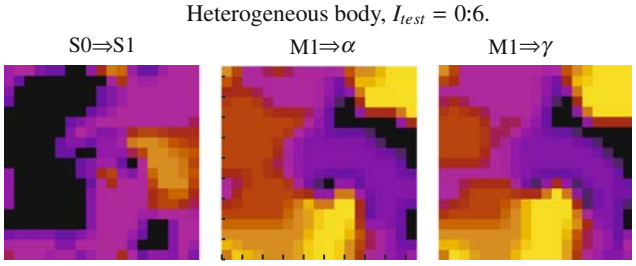

Fig. 17 Self-organization maps of heterogeneous body model. Same *color* map as previous figures

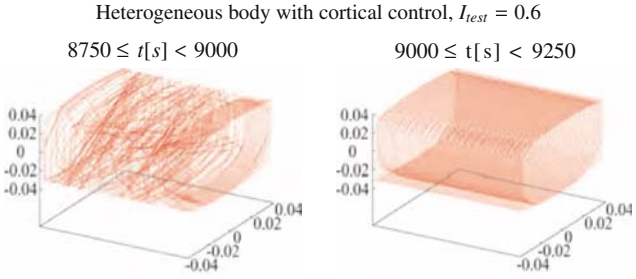

Fig. 18 Characteristic trajectories of heterogeneous body model, while M1 is affecting behavior. Same coordinate system as previous figures

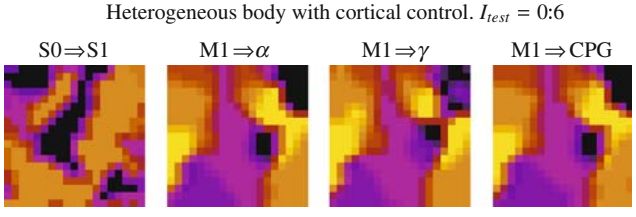

Fig. 19 Self-organization maps of heterogeneous body model, while M1 is affecting behavior. Same *color* map as previous figures

mined to match those of term infant based on literature (Sun and Jensen 1994; Ressler 1977). The joint angle limits are also determined based on literature (Watanabe et al. 1979; Maruyama 2005).

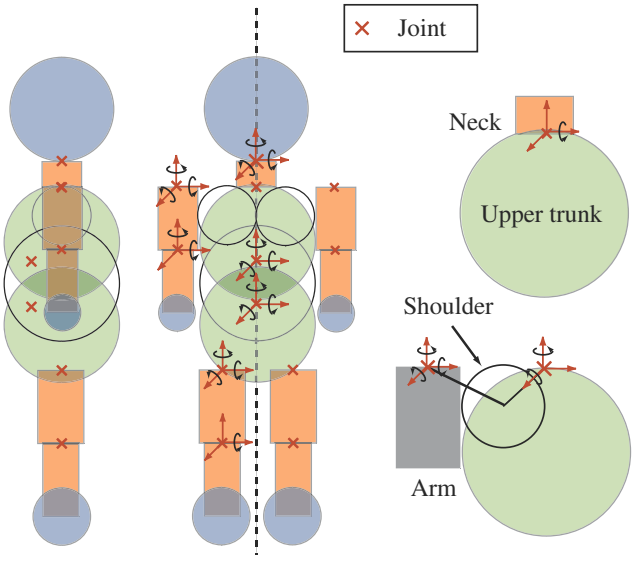

Fig. 20 Skeletal model of fetus and infant

We defined 198 muscles attached to the skeletal model. Finger and face muscles are omitted. Each muscle follows the model given in Sect. 3. The critical muscle parameter is $F_{\max}$, the maximum isometric contraction force. $F_{\max}$ is proportional to the cross-section of the muscle, and its coefficient is reported as 6.3 kgw/cm^3 (Fukunaga 1967). Therefore $F_{\max}$(N) is computed as follows.

$$F_{\max} = 9.8 \cdot 6.3 \cdot \mathrm{PCSA} \tag{27}$$

Here, PCSA cm^2 is the cross-section area of the muscle. PCSA data of infants are very difficult to find. Data for the lower body of infants are found in Spoor et al. (1989). Since we could not find exact data for the upper body of infants, we estimated them from adult data (Freivalds 1985; Friederich and Brand 1990; Smith et al. 1996; Wood et al. 1989a,b), assuming a linear growth of muscle sizes (Scholten et al. 2003).

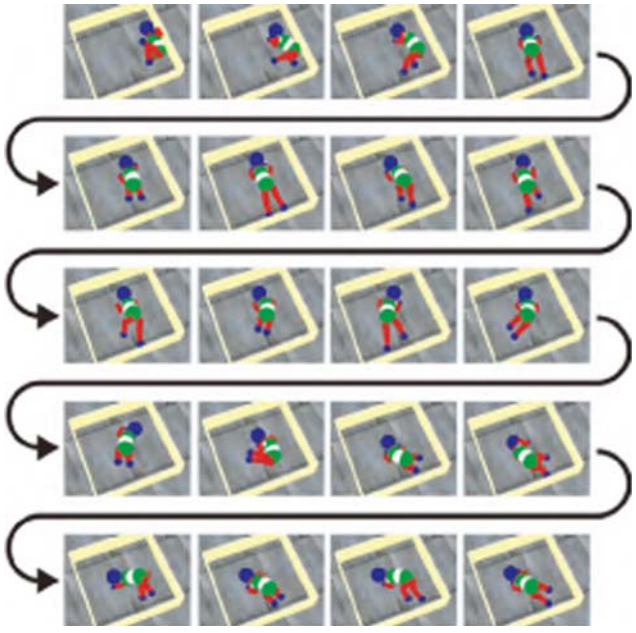

Fig. 21 Emergent behavior of infant model. Rolling over and then starts and continues crawling-like motion

5.2 Preliminary experiments

The body model is connected with the neural model described in Sect. 3 with left and right nervous systems. S1 in each hemisphere has $20 \times 10 = 200$ neurons, and likewise for M1. For each side of the body, 99 each of CPG and spinal neurons are created.

We first tested the model with various I_{test} signals without cortical control. The result was that for $I_{\text{test}} \leq 0.4$ almost no movement was observed, and for large values such as $I_{\text{test}} = 1.0$ the DOF of the movements was very low (only simple bang–bang type of movements). Based on these experiments, we set $I_{\text{test}} = 0.5$ which generates smooth movements with large amplitudes. Then we carried out experiments with the cortical outputs enabled.

The experiments and their analyses are not completed to the conclusive level. We present preliminary results only to show the future possibility of our model.

Figure 21 shows a series of motor behavior observed in one of the experiments. In the figure, the infant model first rolls over from the face up to face down posture, then started to do crawling-like behavior (but without moving forward), which continued for a while. Throughout the experiment, the model often exhibited mixtures of periodic and aperiodic complex movements. The precise cause of the above meaningful behavior must wait for detailed analysis. It is highly plausible to assume that the emergence of meaningful behavior such as crawling owes much to the natural body property; the overall geometry of the skeletal system, natural joint positions due to the natural length settings of the muscles, the intrinsic frequency of the limbs all contribute to the resulting behavior, and the neural system could explore and get entrained into such consistent oscillatory movement as the crawling-like behavior.

6 Discussions and conclusions

As an attempt towards a synthetic understanding of early human motor development, we proposed a principle of spontaneous exploration for embodied motor patterns and learning. A detailed model of neural-body system is presented. It captures the essential features of biological systems, although greatly simplified.

Through a series of experiments with a simple 1-joint model, we showed that the emergent neural-body dynamics has the power to explore and get entrained in various dynamical patterns. By examining the self-organized cortical maps, we identified candidates of motor primitives in terms of alternating muscle contraction patterns. When the learning cortical model is inserted in the motor control loop, a reduction of the complexity of movement is observed after the progress of learning. This phenomenon may correspond to *freezing* of DOFs in early human motor development.

We also presented a preliminary result with a simulated infant body. Some interesting behavior emerged such as rolling-over and crawling-like motion. It is important to note that the model has no pre-defined motor coordination circuit; the only built-in reflex is stretch reflex. Although we have to wait for further experiments and analyses for conclusive results, the above experiment shows the possibility that the model can discover and learn consistent motor patterns exploiting the embodiment.

The presented model is a minimalist version omitting many important factors of biological systems. Our intention is that this version of the model should serve as the baseline for examining the effect of various biological constraints. By introducing one constraint at a time, we expect to find its effect.

Appendix: Details of muscle/spindle model parameters

Muscle model details

Definitions of the variables and the parameters referred in Sect. 3.3 are given below.

v denotes a normalized contraction velocity defined below.

$$v = \frac{0.05\dot{l}}{V_{\max}} \tag{28}$$

Here, $\dot{l}$ is time derivative of l, and $V_{\max}$ is set to 0.250 m/s as defined by He.

In (15), $f_l(l)$ and $f_v(v)$ denote the length dependent and velocity dependent components, respectively, of the normalized active contraction force, defined in the following.

$$f_l(l) = \exp\left(-\left(\frac{|l^{2.8286} - 1|}{0.6182}\right)^{2.3680}\right) \tag{29}$$

$$f_v(v) = \begin{cases} (1+7.3125v)/(1+4.0625v) & (v \geq 0\text{: stretching}) \\ (1+v)/(1-2.25v) & (v < 0\text{: contracting}) \end{cases} \tag{30}$$

$f_p(l)$ and $B_p(l)$ in (15) denote the length dependent and damper components, respectively, of the normalized passive contraction force, defined as follows.

$$f_p(l) = \begin{cases} 0.1663(\exp(208.2(0.05l - 0.036)) - 1) & (0.036 < 0.05l < 0.057) \\ 13.0076 + 2743(0.05l - 0.057) & (0.05l \geq 0.057) \\ 0 & (0.05l \leq 0.036) \end{cases} \tag{31}$$

$$B_p(l) = \begin{cases} 0.34624\exp(208.2(0.05l - 0.036)) & (0.05l < 0.057) \\ 27.4 & (0.05l \geq 0.057) \end{cases} \tag{32}$$

Spindle model details

Definitions of the variables and the parameters referred in Sect. 3.4.1 are given below.

Let f_{vs} the velocity dependent component of the contraction force of the intrafusal muscle fiber, then $\dot{y}$ is represented as follows.

$$\dot{y} = \begin{cases} (1 - f_{vs})/(22.7 \cdot f_{vs} - 85.5) & (f_{vs} > 1) \\ (1 - f_{vs})/(-62.8 \cdot f_{vs} - 1) & (f_{vs} \leq 1) \end{cases} \tag{33}$$

$$f_{vs} = \frac{b \cdot z}{f_{ls}(l_s)} \tag{34}$$

Here, l_s denotes the stretch of the intrafusal muscle fiber, and $f_{ls}(l_s)$ the length dependent component of the contraction force of the intrafusal muscle fiber, defined as follows.

$$f_{ls}(l_s) = \begin{cases} 0.0009197 \cdot \exp(400 \cdot l_s) & (l_s < 0.0025) \\ l_s & (l_s \geq 0.0025) \end{cases} \tag{35}$$

$$l_s = x - z - 0.035 \tag{36}$$

b in (34) is the stiffness ratio of the sensory part to the intrafusal muscle fiber. Denoting the incoming signal to the spindle as i [pulses/s], b is defined as follows.

$$b = b(i) = \frac{99}{1 + 0.08 \cdot i} \tag{37}$$

By feeding i and $\dot{x}$ to the above equations, $\dot{z}$ is obtained, which is then numerically integrated to compute z.

References

Aoi S, Tsuchiya K (2006) Bifurcation and chaos of a simple walking model driven by a rhythmic signal. Int J Non linear Mech 41(3):438–446

Arena P, Caponnetto R, Fortuna L, Rosa ML, Rizzo A (2000) Nonorganized deterministic dissymetries induce regularity in spatiotemporal dynamics. Int J Bifurc Chaos 10(1):73–85

Asai Y, Nomura T, Sato S (2000) Emergence of oscillations in a model of weakly coupled two bonhoeffer van der pol equations. BioSystems 58:239–247

Asai Y, Nomura T, Sato S, Tamaki A, Matsuo Y, Mizukura I, Abe K (2003) A coupled oscillator model of disordered interlimb coordination in patients with parkinson disease. Biol Cybern 88:152–162

Bernstein NA (1996) On dexterity and its development. In: Latash ML, Turvey MT (eds) Dexterity and Its Development, Lawrence Erlbaum Associates pp. 3–44

Chen Y (1997) A motor control model based on self-organizing feature maps. Ph.D. thesis, the University of Maryland

Collins JJ, Richmond SA (1994) Hard-wired central pattern generators for quadrupedal locomotion. Biol Cybern 71(5):375–385

Crair MC (1999) Neuronal activity during development: permissive or instructive? Curr Opin Neurobiol 9:88–93

Freivalds A Incorporation of active elements into the articulated total body model. Paper aamrl-tr-85-061, Armstrong Aerospace Medical Research Laboratory

Friederich JA, Brand RA (1990) Muscle fiber architecture in the human lower limb. J Biomech 23(1):91–95

Fukunaga T (1967) Computation of muscle force per unit muscle cross-section based on ultrasonic measurements (in Japanese). Jpn J Phy Educ 14(1):28–31

Goodall S, Reggia J, Chen Y, Ruppin E, Whitney C (1997) A computational model of acute focal cortical lesions. Stroke 28:101–109

Grillner S et al. (1991) Neuronal network generating locomotor behavior in lamprey: circuitry, transmitters, membrane properties and simulation. Ann Rev Neurosc 14:169–199

Hakamada S, Hayakawa F, Kuno K, Tanaka R (1988) Development of the monosynaptic reflex pathway in the human spinal cord. Dev Brain Res 42:239–246

He J, Maltenfort MG, Wang Q, Hamm TM (2001) Learning from biological systems : modeling neural control. Control Syst Mag 21(4):55–69

Hill AV (1938) The heat of shortening and the dynamic constants of muscle. Proc R Soc Lond B126:136–195

Ijspeert AJ (2001) A connectionist central pattern generator for the aquatic and terrestrial gaits of a simulated salamander. Biol Cybern 84(5):331–348

Inui K, Wang X, Tamura Y, Kaneoke Y, Kakigi R (2004) Serial processing in the human somatosensory system. Cere Cortex 14:851–857

Issler H, Stephens JA (1983) The maturation of cutaneous reflexes studied in the upper limb in man. J Physiol 335:643–654

Johnson MH (2005) Developmental Cognitive Neuroscience, 2nd edn. Blackwell, Oxford

Kaneko K (1984) Period-doubling of kink-antikink patterns, quasi-periodicity in antiferro-like structures and spatial intermittency in coupled map lattices—toward a prelude to a "field theory of chaos". Prog Theor Phys 72:480–486

Kaneko K (1989) Chaotic but regular posi-nega switch among coded attractors by cluster size variation. Phys Rev Lett 63:219

Kaneko K (1990) Clustering, coding, switching, hierarchical ordering, and control in a network of chaotic elements. Physica D 41:137–172

Kaneko K (1994) Relevance of clustering to biological networks. Physica D 77:456

Kaneko K, Tsuda I (2001) Complex Systems: Chaos and Beyond. Springer, Berlin Heidelberg New York

Kimura H, Fukuoka Y, Konaga K (2001) Adaptive dynamic walking of a quadruped robot by using neural system model. Adv Robot 15(8):859–876

Kisilevsky B, Low J (1998) Human fetal behavior: 100 years of study. Dev Rev 18:1–29

Kohonen T (1997) Self-Organizing Maps (2nd edn.). No. 30 in Springer Series in Information Sciences. Springer, Berlin Heidelberg New York

Kuniyoshi Y, Ohmura Y, Terada K, Nagakubo A (2004) Dynamic roll-and-rise motion by an adult-size humanoid robot. Int J Humanoid Robot 1(3):497–516

Kuniyoshi Y, Suzuki S (2004) Dynamic emergence and adaptation of behavior through embodiment as coupled chaotic field. In: Proceedings of IEEE International Conference on Intelligent Robots and Systems, pp. 2042–2049

Kuniyoshi Y et al. (2004) Embodied basis of invariant features in execution and perception of whole body dynamic actions—knacks and focuses of roll-and-rise motion. Robotics and Autonomous Systems 48(4):189–201

Lin CCK, Crago PE (2002) Neural and mechanical contributions to the stretch reflex: a model synthesis. Ann Biomed Eng 30:54–67

Maruyama H (ed) (2005) Clinical Kinesiology, 4th edn (in Japanese). The Society of Physical Therapy Science

Matsumoto K, Tsuda I (1983) Noise-induced order. J Stat Phys 31:87

McGeer T (1990) Passive dynamic walking. Int J Robot Res 9(2):62–82

Morimoto J, Doya K (2001) Acquisition of stand-up behavior by a real robot using hierarchical reinforcement learning. Robot Auton Syst 36(1):37–51

Ott E, Grebogi C, Yorke JA (1990) Controlling chaos. Phys Rev Lett 64(11):1196–1199

Pribe C, Grossberg S, Cohen MA (1997) Neural control of interlimb oscillations ii. biped and quadruped gaits and bifurcations. Biol Cybern 77(2)

Rakic P (1998) Specification of cerebral cortical areas. Science 241:170–176

Ressler S (1977) Anthrokids—anthropometric data of children http://www.itl.nist.gov/iaui/ovrt/projects/anthrokids/

Rizzi AA, Koditschek DE (1993) Further progress in robot juggling: The spatial two-juggle. In: Proceedings of IEEE International Conference on Robotics and Automation, pp. 919–924

Sarnat HB (2003) Functions of the corticospinal and corticobulbar tracts in the human newborn. J. of Pediat. Neurol. 1(1):3–8

Sato M, Nakamura Y, Ishii S (2002) Reinforcement Learning for Biped Locomotion, *Lecture Notes in Computer Science*, vol 2415/2002 Springer, Berlin Heidelberg New York p. 777

Scholten RR, Pillen S, Verrips A, Zwarts MJ (2003) Quantitative ultrasonography of skeletal muscles in children: Normal values. Muscle Nerve 27:693–698

Shue G, Crago PE (1998) Muscle-tendon model with length history-dependent activation-velocity coupling. Ann Biomed Eng 26:369–380

Small M, Judd K, Lowe M, Stick S (1999) Is breathing in infants chaotic? dimension estimates for respiratory patterns during quiet sleep. J Appl Physiol 86:359–376

Smith LK, Weiss EL, Lehmkuhl DL (1996) Brunnstrom's Clinical Kinesiology. F.A. Davis Co

Spoor CW, van Leeuwen JL, de Windt FH, Huson A (1989) a model study of muscle forces and joint-force direction in normal and dysplastic neonatal hips. J Biomech 22(8–9):873–884

Sun H, Jensen R (1994) Body segment growth during infancy. J Biomech 21(3):265–275

Taga G (1994) Emergence of bipedal locomotion through entrainment among the neuromusculo-skeletal system and the environment. Physica D 75(1-3):190–208

Taga G, Takaya R, Konishi Y (1999) Analysis of general movements of infants towards understanding of developmental principle for motor control. In: Proceedings of IEEE International Conference on Systems, Man, Cybernetics, vol 5, pp 678–683 (1999)

Taga G, Yamaguchi Y, Shimizu H (1991) Self-organized control of bipedal locomotion in unpredictable environment. Biol. Cybern 65:147–159

Tsuda I (1991) Chaotic itinerancy as a dynamical basis of hermeneutics in brain and mind. World Futures 32, 167 (1991)

Watanabe H, Ogata K, Ogata T (1979) On mobile range of four limbs of normal japanese—variation with age (in Japanese). J Jpn Orthop Assoc 53(3):275–291

Wisse M, van Frankenhuyzen J (2006) Design and construction of mike; a 2-D autonomous biped based on passive dynamic walking. In: Kimura H, Tsuchiya K, Ishiguro A, Witte H (eds) Adaptive Motion of Animals and Machines, vol 4, Springer, Tokyo pp 143–154

Wood JE, Meek SG, Jacobsen SC (1989a) Quantitation of human shoulder anatomy for prosthetic arm control—i. surface modelling. J Biomech 22(3):273–292

Wood JE, Meek SG, Jacobsen SC (1989b) Quantitation of human shoulder anatomy for prosthetic arm control–ii. anatomy matrices. J Biomech 22(4):309–325

Yang Z, França FMG (2003) A generalized locomotion cpg architecture based on oscillatory building blocks. Biol Cybern 89(1):34–42